7

Models and Theories of Nuclear Physics

Nuclei are held together by the strong nuclear force between nucleons, so we start this chapter by looking at the form of this, which is more complicated than that generated by simple one-particle exchange. Much of the phenomenological evidence comes from low-energy nucleon–nucleon scattering experiments which we will simply quote, but we will interpret the results in terms of the fundamental strong interaction between quarks. The rest of the chapter is devoted to various models and theories that are constructed to explain nuclear data in particular domains.

7.1 The Nucleon – Nucleon Potential

The existence of stable nuclei implies that overall the net nucleon–nucleon force must be *attractive* and much stronger than the Coulomb force, although it cannot be attractive for all separations, or otherwise nuclei would collapse in on themselves. So at very short ranges there must be a repulsive core. However, the repulsive core can be ignored in low-energy nuclear structure problems because low-energy particles cannot probe the short-distance behaviour of the potential. In lowest order, the potential may be represented dominantly by a central term (i.e. one that is a function only of the radial separation of the particles), although there is also a smaller non-central part. We know from proton–proton scattering experiments[1] that the nucleon–nucleon force is *short-range*, of the same order as the size of the nucleus, and thus does not correspond to the exchange of gluons, as in the fundamental strong interaction. A schematic diagram of the resulting potential is shown in Figure 7.1. In practice of course this strong

[1]For reviews see, for example, Chapter 7 of Je90 and Chapter 14 of Ho97.

Nuclear and Particle Physics B. R. Martin
 ISBN: 0-470-01999-9

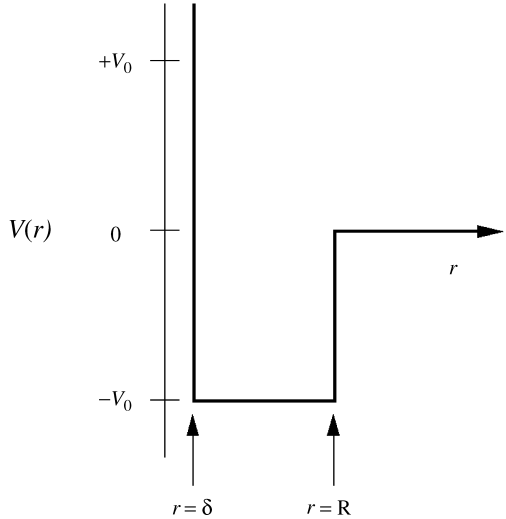

Figure 7.1 Idealized square well representation of the strong interaction nucleon--nucleon potential. The distance R is the range of the nuclear force and $\delta \ll R$ is the distance at which the short-range repulsion becomes important. The depth V_0 is approximately 40 MeV

interaction potential must be combined with the Coulomb potential in the case in the case of protons.

A comparison of *nn* and *pp* scattering data (after allowing for the Coulomb interaction) shows that the nuclear force is *charge-symmetric* ($pp = nn$) and almost *charge-independent* ($pp = nn = pn$).[2] We have commented in Chapter 3 that there is also evidence for this from nuclear physics. Charge-symmetry is seen in comparisons of the energy levels of mirror nuclei (see, for example, Figure 3.9) and evidence for charge-independence comes from the energy levels of triplets of related nuclei with the same A values. Nucleon–nucleon forces are, however, *spin-dependent*. The force between a proton and neutron in an overall spin-1 state (i.e. with spins parallel) is strong enough to support a weakly bound state (the *deuteron*), whereas the potential corresponding to the spin-0 state (i.e. spins antiparallel) has no bound states. Finally, nuclear forces *saturate*. This describes that fact that a nucleon in a typical nucleus experiences attractive interactions only with a limited number of the many other nucleons and is a consequence of the short-range nature of the force. The evidence for this is the form of the nuclear binding energy curve and was discussed in Chapter 2.

Ideally one would like to be able to interpret the nucleon–nucleon potential in terms of the fundamental strong quark–quark interactions. It is not yet possible to give a complete explanation along these lines, but it is possible to go some way in this direction. If we draw an analogy with atomic and molecular structure, with

[2]For a discussion of these data see, for example, the references in Footnote 1.

quarks playing the role of electrons, then possibilities are: an ionic-type bond, a van der Waals type of force, or a covalent bond.[3] The first can be ruled out because the confining forces are too strong to permit a quark to be 'lent' from one nucleon to another and the second can also be ruled out because the resulting two-gluon exchange is too weak. This leaves a covalent bond due to the sharing of single quarks between the nucleons analogous to the covalent bond that binds the hydrogen molecule. However, nucleons have to remain 'colourless' during this process and so the shared quark from one nucleon has to have the same colour as the shared quark from the other nucleon. The effect of this is to reduce the effective force (because there are three possible colour states) and by itself it is unable to explain the depth of the observed potential. In addition to the three (valence) quarks within the nucleon there are also present quark–antiquark pairs due to vacuum fluctuations.[4] Such pairs can be colourless and so can also be shared between the nucleons. These quarks actually play a greater role in generating the nuclear strong interaction than single quarks. The lightest such diquarks will be pions and this exchange gives the largest contribution to the attractive part of the nucleon–nucleon force (see, for example, the Feynman diagram Figure 1.4).

In principle, the short-range repulsion could be due to the exchange of heavier diquarks (i.e. mesons), possibly also in different overall spin states. Experiment provides many suitable meson candidates, in agreement with the predictions of the quark model, and each exchange would give rise to a specific contribution to the overall nucleon–nucleon potential, by analogy with the Yukawa potential resulting from the exchange of a spin-0 meson, as discussed in Chapter 1. It is indeed possible to obtain excellent fits to nucleon–nucleon scattering data in a model with several such exchanges.[5] Thus this approach can yield a satisfactory potential model, but is semi-phenomenological only, as it requires the couplings of each of the exchanged particles to be found by fitting nucleon–nucleon scattering data. (The couplings that result broadly agree with values found from other sources.) Boson-exchange models therefore cannot give a fundamental explanation of the repulsion. The reason for the repulsion at small separations in the quark model lies in the spin dependence of the quark–quark strong interaction, which like the phenomenological nucleon–nucleon interaction, is strongly spin-dependent. We have discussed this in the context of calculating hadron masses in Section 3.3.3. When the two nucleons are very close, the wavefunction is effectively that for a 6-quark system with zero angular momentum between the quarks, i.e. a symmetric spatial wave function. Since the colour wave function is antisymmetric, (recall the discussion of Chapter 5), it follows that the spin wavefunction is symmetric. However, the

---

[3]Recall from chemistry that in ionic bonding, electrons are permanently transferred between constituents to form positive and negative ions that then bind by electrostatic attraction; in covalent bonding the constituents share electrons; and the van der Waals force is generated by the attraction between temporary charges induced on the constituents by virtue of slight movements of the electrons.

[4]These are the 'sea' quarks mentioned in connection with the quark model in Chapter 3 and which are probed in deep inelastic lepton scattering that was discussed in Chapter 6.

[5]This approach is discussed in, for example, Chapter 3 of Co01 and also in the references given in Footnote1.

potential energy increases if all the quarks remain in the $L = 0$ state with spins aligned.[6] The two-nucleon system will try to minimize its 'chromomagnetic' energy, but this will compete with the need to have a symmetric spin wavefunction. The optimum configuration at small separations is when one pair of quarks is in an $L = 1$ state, although the excitation energy is comparable to the decrease in chromomagnetic energy, so there will still be a net increase in energy at small separations.

Some tantalizing clues exist about the role of the quark–gluon interaction in nuclear interactions, such as the small nuclear effects in deep inelastic lepton scattering mentioned in Chapter 5. There is also a considerable experimental programme in existence (for example at CEBAF, the superconducting accelerator facility at the Jefferson Laboratory, Virginia, USA, mentioned in Chapter 4) to learn more about the nature of the strong nucleon–nucleon force in terms of the fundamental quark–gluon strong interaction and further progress in this area may well result in the next few years. Meanwhile, in the absence of a fundamental theory to describe the nuclear force, specific models and theories are used to interpret the phenomena in different areas of nuclear physics. In the remainder of this chapter we will discuss a number of such approaches.

7.2 Fermi Gas Model

In this model, the protons and neutrons that make up the nucleus are assumed to comprise two independent systems of nucleons, each freely moving inside the nuclear volume subject to the constraints of the Pauli principle. The potential felt by every nucleon is the superposition of the potentials due to all the other nucleons. In the case of neutrons this is assumed to be a finite-depth square well; for protons, the Coulomb potential modifies this. A sketch of the potential wells in both cases is shown in Figure 7.2.

For a given ground state nucleus, the energy levels will fill up from the bottom of the well. The energy of the highest level that is completely filled is called the *Fermi level* of energy E_F and has a momentum $p_F = (2ME_F)^{1/2}$, where M is the mass of the nucleon. Within the volume V, the number of states with a momentum between p and $p + dp$ is given by the *density of states factor*

$$n(p)\mathrm{d}p = \mathrm{d}n = \frac{4\pi V}{(2\pi\hbar)^3} p^2 \mathrm{d}p, \tag{7.1}$$

[6] Compare the mass of the $\Delta(1232)$ resonance, where all three quarks spins are aligned, to that of the lighter nucleon, where one pair of quarks spins is anti-aligned to give a total spin of zero. This is discussed in detail in Section 3.3.3.

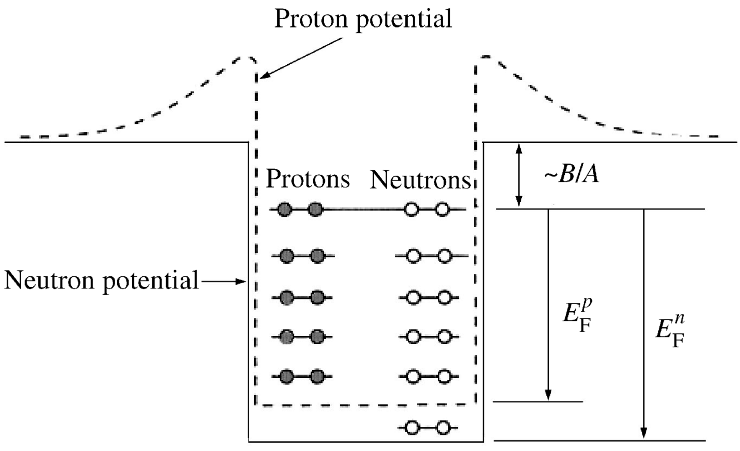

Figure 7.2 Proton and neutron potentials and states in the Fermi gas model

which is derived in Appendix A. Since every state can contain two fermions of the same species, we can have (using $n = 2\int_0^{p_F} dn$)

$$N = \frac{V(p_F^n)^3}{3\pi^2\hbar^3} \quad \text{and} \quad Z = \frac{V(p_F^p)^3}{3\pi^2\hbar^3} \tag{7.2}$$

neutrons and protons, respectively, with a nuclear volume

$$V = \frac{4}{3}\pi R^3 = \frac{4}{3}\pi R_0^3 A, \tag{7.3}$$

where experimentally $R_0 = 1.21$ fm, as we have seen from electron and hadron scattering experiments discussed in Chapter 2. Assuming for the moment that the depths of the neutron and proton wells are the same, we find for a nucleus with $Z = N = A/2$, the Fermi momentum

$$p_F = p_F^n = p_F^p = \frac{\hbar}{R_0}\left(\frac{9\pi}{8}\right)^{1/3} \approx 250\,\text{MeV/c}. \tag{7.4}$$

Thus the nucleons move freely within the nucleus with quite large momenta.

The Fermi energy is

$$E_F = \frac{p_F^2}{2M} \approx 33\,\text{MeV}. \tag{7.5}$$

The difference between the top of the well and the Fermi level is constant for most heavy nuclei and is just the average binding energy per nucleon

$\tilde{B} \equiv B/A = 7$–8 MeV. The depth of the potential and the Fermi energy are to a good approximation independent of the mass number A:

$$V_0 = E_{\rm F} + \tilde{B} \approx 40\,{\rm MeV}. \tag{7.6}$$

Heavy nuclei generally have a surplus of neutrons. Since the Fermi levels of the protons and neutrons in a stable nucleus have to be equal (otherwise the nucleus can become more stable by β-decay) this implies that the depth of the potential well for the neutron gas has to be deeper than for the proton gas, as shown in Figure 7.2. Protons are therefore on average less tightly bound in nuclei than are neutrons.

We can use the Fermi gas model to give a theoretical expression for some of the dependence of the binding energy on the surplus of neutrons, as follows. First, we define the average kinetic energy per nucleon as

$$\langle E_{\rm kin}\rangle \equiv \left[\int_0^{p_{\rm F}} E_{\rm kin} p^2 {\rm d}p\right]\left[\int_0^{p_{\rm F}} p^2 {\rm d}p\right]^{-1}. \tag{7.7}$$

Evaluating the integrals gives

$$\langle E_{\rm kin}\rangle = \frac{3}{5}\frac{p_{\rm F}^2}{2M} \approx 20\,{\rm MeV}. \tag{7.8}$$

The total kinetic energy of the nucleus is then

$$E_{\rm kin}(N,Z) = N\langle E_n\rangle + Z\langle E_p\rangle = \frac{3}{10\,M}\left[N(p_{\rm F}^n)^2 + Z(p_{\rm F}^p)^2\right], \tag{7.9}$$

which may be re-expressed as

$$E_{\rm kin}(N,Z) = \frac{3}{10\,M}\frac{\hbar^2}{R_0^2}\left(\frac{9\pi}{4}\right)^{2/3}\left[\frac{N^{5/3}+Z^{5/3}}{A^{2/3}}\right], \tag{7.10}$$

where again we have taken the radii of the proton and neutron wells to be equal. This expression is for fixed A but varying N and has a minimum at $N = Z$. Hence the binding energy gets smaller for $N \neq Z$. If we set $N = (A+\Delta)/2$, $Z = (A-\Delta)/2$, where $\Delta \equiv N - Z$, and expand Equation (7.10) as a power series in Δ/A, we obtain

$$E_{\rm kin}(N,Z) = \frac{3}{10\,M}\frac{\hbar^2}{R_0^2}\left(\frac{9\pi}{8}\right)^{2/3}\left[A + \frac{5}{9}\frac{(N-Z)^2}{A} + \ldots\right], \tag{7.11}$$

which gives the dependence on the neutron excess. The first term contributes to the volume term in the semi-empirical mass formula (SEMF), while the second describes the correction that results from having $N \neq Z$. This is a contribution to the asymmetry term we have met before in the SEMF and grows as the square of the neutron excess. Evaluating this term from Equation (7.11) shows that its contribution to the asymmetry coefficient defined in Equation (2.51) is about 44 $\mathrm{MeV/c^2}$, compared with the empirical value of about 93 $\mathrm{MeV/c^2}$ given in Equation (2.54). In practice, to reproduce the actual term in the SEMF accurately we would have to take into account the change in the potential energy for $N \neq Z$.

7.3 Shell Model

The nuclear shell model is based on the analogous model for the orbital structure of atomic electrons in atoms. In some areas it gives more detailed predictions than the Fermi gas model and it can also address questions that the latter model cannot. Firstly, we recap the main features of the atomic case.

7.3.1 Shell structure of atoms

The binding energy of electrons in atoms is due primarily to the central Coulomb potential. This is a complicated problem to solve in general because in a multi-electron atom we have to take account of not only the Coulomb field of the nucleus, but also the fields of all the other electrons. Analytic solutions are not usually possible. However, many of the general features of the simplest case of hydrogen carry over to more complicated cases, so it is worth recalling the former.

Atomic energy levels are characterized by a quantum number $n = 1, 2, 3, 4, \ldots.$ called the *principal quantum number*. This is defined so that it determines the energy of the system.[7] For any n there are energy-degenerate levels with *orbital angular momentum quantum numbers* given by

$$\ell = 0, 1, 2, 3, \ldots, (n-1) \tag{7.12}$$

(this restriction follows from the form of the Coulomb potential) and for any value of ℓ there are $(2\ell + 1)$ sub-states with different values of the projection of orbital angular momentum along any chosen axis (the *magnetic quantum number*):

$$m_\ell = -\ell, -\ell + 1, \ldots, 0, 1, \ldots, \ell - 1, \ell. \tag{7.13}$$

Due to the rotational symmetry of the Coulomb potential, all such sub-states are degenerate in energy. Furthermore, since electrons have spin-$\frac{1}{2}$, each of the above

[7] In nuclear physics we are not dealing with the same simple Coulomb potential, so it would be better to call n the *radial node quantum number*, as it still determines the form of the radial part of the wavefunction.

states can be occupied by an electron with spin 'up' or 'down', corresponding to the *spin-projection quantum number*

$$m_s = \pm 1/2. \tag{7.14}$$

Again, both these states will have the same energy. So finally, any energy eigenstate in the hydrogen atom is labelled by the quantum numbers (n, ℓ, m_ℓ, m_s) and for any n, there will be n_{d} degenerate energy states, where

$$n_{\mathrm{d}} = 2\sum_{\ell=0}^{n-1}(2\ell + 1) = 2n^2. \tag{7.15}$$

The high degree of degeneracy can be broken if there is a preferred direction in space, such as that supplied by a magnetic field, in which case the energy levels could depend on m_ℓ and m_s. One such interaction is the spin–orbit coupling, which is the interaction between the magnetic moment of the electron (due to its spin) and the magnetic field due to the motion of the nucleus (in the electron rest frame). This leads to corrections to the energy levels called *fine structure*, the size of which are determined by the electromagnetic fine structure constant α.

In atomic physics the fine-structure corrections are small and so, if we ignore them for the moment, in hydrogen we would have a system with electron orbits corresponding to shells of a given n, with each shell having degenerate sub-shells specified by the orbital angular momentum ℓ. Going beyond hydrogen, we can introduce the electron–electron Coulomb interaction. This leads to a splitting in any energy level n according to the ℓ value. The degeneracies in m_l and m_s are unchanged. It is straightforward to see that if a shell or sub-shell is filled, then we have

$$\sum m_s = 0 \quad \text{and} \quad \sum m_\ell = 0, \tag{7.16}$$

i.e. there is a strong pairing effect for closed shells. In these cases it can be shown that the Pauli principle implies

$$\mathbf{L} = \mathbf{S} = \mathbf{0} \quad \text{and} \quad \mathbf{J} = \mathbf{L} + \mathbf{S} = \mathbf{0}. \tag{7.17}$$

For any atom with a closed shell or a closed sub-shell structure, the electrons are paired off and thus no valence electrons are available. Such atoms are therefore chemically inert. It is straightforward to work out the atomic numbers at which this occurs. These are

$$Z = 2, 10, 18, 36, 54. \tag{7.18}$$

For example, the inert gas argon $\mathrm{Ar}(Z = 18)$ has closed shells corresponding to $n = 1$, 2 and closed sub-shells corresponding to $n = 3, \ell = 0, 1$. These values of Z are called the *atomic magic numbers*.

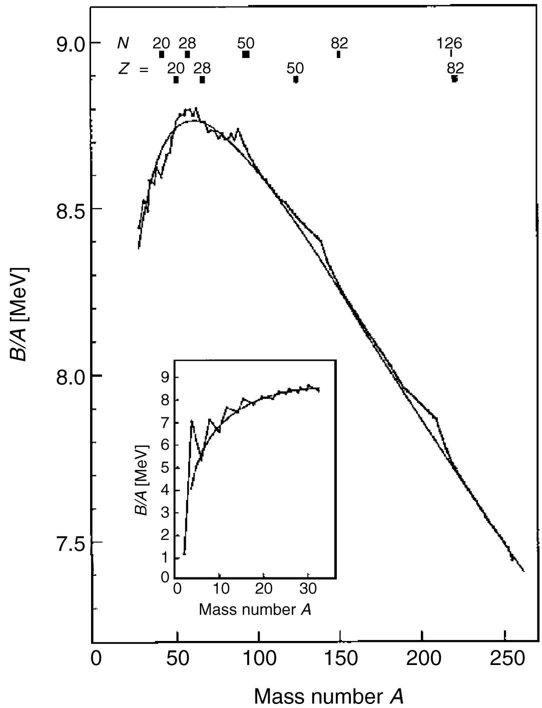

Figure 7.3 Binding energy per nucleon for even values of A: the solid curve is the SEMF (from Bo69)

7.3.2 Nuclear magic numbers

In nuclear physics, there is also evidence for magic numbers, i.e. values of Z and N at which the nuclear binding is particularly strong. This can been seen from the B/A curves of Figure 2.10 where at certain values of N and Z the data lie above the SEMF curve. This is also shown in Figure 7.3, where the inset shows the low-A region magnified. (The figure only shows results for even values of the mass number A.)

The *nuclear magic numbers* are found from experiment to be

$$\begin{aligned} N &= 2, 8, 20, 28, 50, 82, 126 \\ Z &= 2, 8, 20, 28, 50, 82 \end{aligned} \tag{7.19}$$

and correspond to one or more closed shells, plus eight nucleons filling the s and p sub-shells of a nucleus with a particular value of n. Nuclei with both N and Z having one of these values are called *doubly magic*, and have even greater stability. An example is the helium nucleus, the α-particle.

Shell structure is also suggested by a number of other phenomena. For example: 'magic' nuclei have many more stable isotopes than other nuclei; they have very small electric dipole moments, which means they are almost spherical, the most tightly bound shape; and neutron capture cross-sections show sharp drops compared with neighbouring nuclei. However, to proceed further we need to know something about the effective potential.

A simple Coulomb potential is clearly not appropriate and we need some form that describes the effective potential of all the other nucleons. Since the strong nuclear force is short-ranged we would expect the potential to follow the form of the density distribution of nucleons in the nucleus. For medium and heavy nuclei, we have seen in Chapter 2 that the Fermi distribution fits the data and the corresponding potential is called the *Woods–Saxon* form

$$V_{\text{central}}(r) = \frac{-V_0}{1 + e^{(r-R)/a}}. \tag{7.20}$$

However, although these potentials can be shown to offer an explanation for the lowest magic numbers, they do not work for the higher ones. This is true of all purely central potentials.

The crucial step in understanding the origin of the magic numbers was taken in 1949 by Mayer and Jensen who suggested that by analogy with atomic physics there should also be a spin–orbit part, so that the total potential is

$$V_{\text{total}} = V_{\text{central}}(r) + V_{\ell s}(r)\mathbf{L}\cdot\mathbf{S}, \tag{7.21}$$

where **L** and **S** are the orbital and spin angular momentum operators for a single nucleon and $V_{\ell s}(r)$ is an arbitrary function of the radial coordinate.[8] This form for the total potential is the same as that used in atomic physics except for the presence of the function $V_{\ell s}(r)$. Once we have coupling between **L** and **S** then m_ℓ and m_s are no longer 'good' quantum numbers and we have to work with eigenstates of the total angular momentum vector **J**, defined by $\mathbf{J} = \mathbf{L} + \mathbf{S}$. Squaring this, we have

$$\mathbf{J}^2 = \mathbf{L}^2 + \mathbf{S}^2 + 2\mathbf{L}\cdot\mathbf{S}, \tag{7.22}$$

i.e.

$$\mathbf{L}\cdot\mathbf{S} = \frac{1}{2}(\mathbf{J}^2 - \mathbf{L}^2 - \mathbf{S}^2) \tag{7.23}$$

and hence the expectation value of $\mathbf{L}\cdot\mathbf{S}$, which we write as $\langle \ell s \rangle$, is

$$\langle \ell s \rangle = \frac{\hbar^2}{2}[j(j+1) - \ell(\ell+1) - s(s+1)] = \begin{cases} \ell/2 & \text{for} \quad j = \ell + \frac{1}{2} \\ -(\ell+1)/2 & \text{for} \quad j = \ell - \frac{1}{2} \end{cases}. \tag{7.24}$$

[8] For their work on the shell structure of nuclei. Maria Goeppert-Mayer and J. Hans Jensen were awarded a half share of the 1963 Nobel Prize in Physics. (They shared the prize with Wigner, mentioned in Chapter 1 for his development of the concept of parity.)

(We are always dealing with a single nucleon, so that $s = \frac{1}{2}$.) The splitting between the two levels is thus

$$\Delta E_{ls} = \frac{2\ell + 1}{2} \hbar^2 \langle V_{\ell s} \rangle. \tag{7.25}$$

Experimentally, it is found that $V_{\ell s}(r)$ is negative, which means that the state with $j = \ell + \frac{1}{2}$ has a lower energy than the state with $j = \ell - \frac{1}{2}$. This is the opposite of the situation in atoms. Also, the splittings are substantial and increase linearly with ℓ. Hence for higher ℓ, crossings between levels can occur. Namely, for large ℓ, the splitting of any two neighbouring degenerate levels can shift the $j = \ell - \frac{1}{2}$ state of the initial lower level to lie above the $j = \ell + \frac{1}{2}$ level of the previously higher level.

An example of the resulting splittings up to the $1G$ state is shown in Figure 7.4, where the usual atomic spectroscopic notation has been used, i.e. levels are written $n\ell_j$ with $S, P, D, F, G, \ldots$. used for $\ell = 0, 1, 2, 3, 4, \ldots$. Magic numbers occur when there are particularly large gaps between groups of levels. Note that there is no restriction on the values of ℓ for a given n because, unlike in the atomic case, the strong nuclear potential is not Coulomb-like.

The *configuration* of a real nuclide (which of course has both neutrons and protons) describes the filling of its energy levels (sub-shells), for protons and for neutrons, in order, with the notation $(n\ell_j)^k$ for each sub-shell, where k is the occupancy of the given sub-shell. Sometimes, for brevity, the completely filled

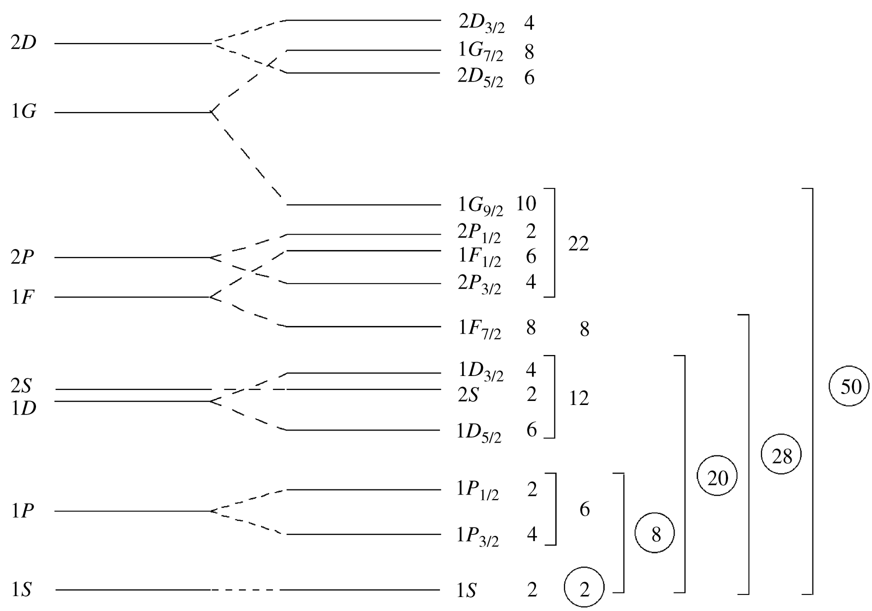

Figure 7.4 Low-lying energy levels in a single-particle shell model using a Woods--Saxon potential plus spin--orbit term; circled integers correspond to nuclear magic numbers

sub-shells are not listed, and if the highest sub-shell is nearly filled, k can be given as a negative number, indicating how far from being filled that sub-shell is. Using the ordering diagram above, and remembering that the maximum occupancy of each sub-shell is $2j + 1$, we predict, for example, the configuration for $^{17}_{8}\mathrm{O}$ to be:

$$(1s_{\frac{1}{2}})^2(1p_{\frac{3}{2}})^4(1p_{\frac{1}{2}})^2 \quad \text{for the protons} \tag{7.26a}$$

and

$$(1s_{\frac{1}{2}})^2(1p_{\frac{3}{2}})^4(1p_{\frac{1}{2}})^2(1d_{\frac{5}{2}})^1 \quad \text{for the neutrons.} \tag{7.26b}$$

Notice that all the proton sub-shells are filled, and that all the neutrons are in filled sub-shells except for the last one, which is in a sub-shell on its own. Most of the ground state properties of $^{17}_{8}\mathrm{O}$ can therefore be found from just stating the neutron configuration as $(1d_{\frac{5}{2}})^1$.

7.3.3 Spins, parities and magnetic dipole moments

The nuclear shell model can be used to make predictions about the *spins* of ground states. A filled sub-shell must have zero total angular momentum, because j is always an integer-plus-a-half, so the occupancy of the sub-shell, $2j + 1$, is always an even number. This means that in a filled sub-shell, for each nucleon of a given $m_j (= j_z)$ there is another having the opposite m_j. Thus the pair have a combined m_j of zero and so the complete sub-shell will also have zero m_j. Since this is true whatever axis we choose for z, the total angular momentum must also be zero. Since magic number nuclides have closed sub-shells, such nuclides are predicted to have zero contribution to the nuclear spin from the neutrons or protons or both, whichever are magic numbers. Hence magic-Z/magic-N nuclei are predicted to have zero nuclear spin. This is indeed found to be the case experimentally.

In fact it is found that *all* even-Z/even-N nuclei have zero nuclear spin. We can therefore make the hypothesis that for ground state nuclei, pairs of neutrons and pairs of protons in a given sub-shell *always* couple to give a combined angular momentum of zero, even when the sub-shell is not filled. This is called the *pairing hypothesis*. We can now see why it is the last proton and/or last neutron that determines the net nuclear spin, because these are the only ones that may not be paired up. In odd-A nuclides there is only one unpaired nucleon, so we can predict precisely what the nuclear spin will be by referring to the filling diagram. For even-A/odd-Z/odd-N nuclides, however, we will have both an unpaired proton and an unpaired neutron. We cannot then make a precise prediction about the net spin because of the vectorial way that angular momenta combine; all we can say is that the nuclear spin will lie in the range $|j_p - j_n|$ to $(j_p + j_n)$.

Predictions can also be made about nuclear *parities*. First, recall the following properties of parity: (1) parity is the transformation $\mathbf{r} \to -\mathbf{r}$; (2) the wavefunction of a single-particle quantum state will contain an angular part proportional to the spherical harmonic $Y^l_m(\theta, \phi)$, and under the parity transformation

$$PY^l_m(\theta,\phi) = (-)^\ell Y^l_m(\theta,\phi); \tag{7.27}$$

(3) a single-particle state will also have an *intrinsic parity*, which for nucleons is defined to be positive. Thus the parity of a single-particle nucleon state depends exclusively on the orbital angular momentum quantum number with $P = (-1)^\ell$. The total parity of a multiparticle state is the *product* of the parities of the individual particles. A pair of nucleons with the same ℓ will therefore always have a combined parity of $+1$. The pairing hypothesis then tells us that the total parity of a nucleus is found from the product of the parities of the last proton and the last neutron. So we can predict the parity of *any* nuclide, including the odd/odd ones, and these predictions are in agreement with experiment.

Unless the nuclear spin is zero, we expect nuclei to have *magnetic (dipole) moments*, since both the proton and the neutron have intrinsic magnetic moments, and the proton is electrically charged, so it can produce a magnetic moment when it has orbital motion. The shell model can make predictions about these moments. Using a notation similar to that used in atomic physics, we can write the nuclear magnetic moment as

$$\mu = g_j\, j\mu_\mathrm{N}, \tag{7.28}$$

where μ_N is the *nuclear magneton* that was used in the discussion of hadron magnetic moments in Section 3.3.3, g_j is the *Landé g-factor* and j is the nuclear spin quantum number. For brevity we can write simply $\mu = g_j\, j$ nuclear magnetons.

We will find that the shell model does not give very accurate predictions for magnetic moments, even for the even–odd nuclei where there is only a single unpaired nucleon in the ground state. We will therefore not consider at all the much more problematic case of the odd–odd nuclei having an unpaired proton and an unpaired neutron.

For the even–odd nuclei, we would expect all the paired nucleons to contribute zero net magnetic moment, for the same reason that they do not contribute to the nuclear spin. Predicting the nuclear magnetic moment is then a matter of finding the correct way to combine the orbital and intrinsic components of magnetic moment of the single unpaired nucleon. We need to combine the spin component of the moment, $g_s s$, with the orbital component, $g_\ell \ell$ (where g_s and g_ℓ are the g-factors for spin and orbital angular momentum.) to give the total moment $g_j\, j$. The general formula for doing this is[9]

$$g_j = \frac{j(j+1) + \ell(\ell+1) - s(s+1)}{2j(j+1)} g_\ell + \frac{j(j+1) - \ell(\ell+1) + s(s+1)}{2j(j+1)} g_s, \tag{7.29}$$

[9]See, for example, Section 6.6 of En66.

which simplifies considerably because we always have $j = \ell \pm \frac{1}{2}$. Thus

$$jg_j = g_\ell \ell + g_s/2 \quad \text{for} \quad j = \ell + \tfrac{1}{2} \tag{7.30a}$$

and

$$jg_j = g_\ell j\left(1 + \frac{1}{2\ell+1}\right) - g_s j\left(\frac{1}{2\ell+1}\right) \quad \text{for} \quad j = \ell - \tfrac{1}{2}. \tag{7.30b}$$

Since $g_\ell = 1$ for a proton and 0 for a neutron, and g_s is approximately $+5.6$ for the proton and -3.8 for the neutron, Equations (7.30) yield the results (where $g_{\text{proton(neutron)}}$ is the g-factor for nuclei with an odd proton(neutron))

$$\begin{aligned}
jg_{\text{proton}} &= \ell + \frac{1}{2} \times 5.6 = j + 2.3 \quad \text{for} \quad j = \ell + \tfrac{1}{2} \\
jg_{\text{proton}} &= j\left(1 + \frac{1}{2\ell+1}\right) - 5.6 \times j\left(\frac{1}{2\ell+1}\right) = j - \frac{2.3j}{j+1} \quad \text{for} \quad j = \ell - \tfrac{1}{2} \\
jg_{\text{neutron}} &= -\frac{1}{2} \times 3.8 = -1.9 \quad \text{for} \quad j = j = \ell + \tfrac{1}{2} \\
jg_{\text{neutron}} &= 3.8 \times j\left(\frac{1}{2\ell+1}\right) = \frac{1.9j}{j+1} \quad \text{for} \quad j = \ell - \tfrac{1}{2}.
\end{aligned} \tag{7.31}$$

Accurate values of magnetic dipole moments are available for a wide range of nuclei and plots of a sample of measured values for a range of odd-Z and odd-N nuclei across the whole periodic table are shown in Figure 7.5. It is seen that for a given j, the measured moments usually lie somewhere between the $j = \ell - \frac{1}{2}$ and the $j = \ell + \frac{1}{2}$ values (the so-called *Schmidt lines*), but beyond that the model does not predict the moments accurately. The only exceptions are a few low-A nuclei where the numbers of nucleons are close to magic values.

Why should the shell model work so well when predicting nuclear spins and parities, but be poor for magnetic moments? There are several likely problem areas, including the possibility that protons and neutrons inside nuclei may have effective intrinsic magnetic moments that are different to their free-particle values, because of their very close proximity to one another.

7.3.4 Excited states

In principle, the shell model's energy level structure can be used to predict nuclear excited states. This works quite well for the first one or two excited states when there is only one possible configuration of the nucleus. However, for higher states the

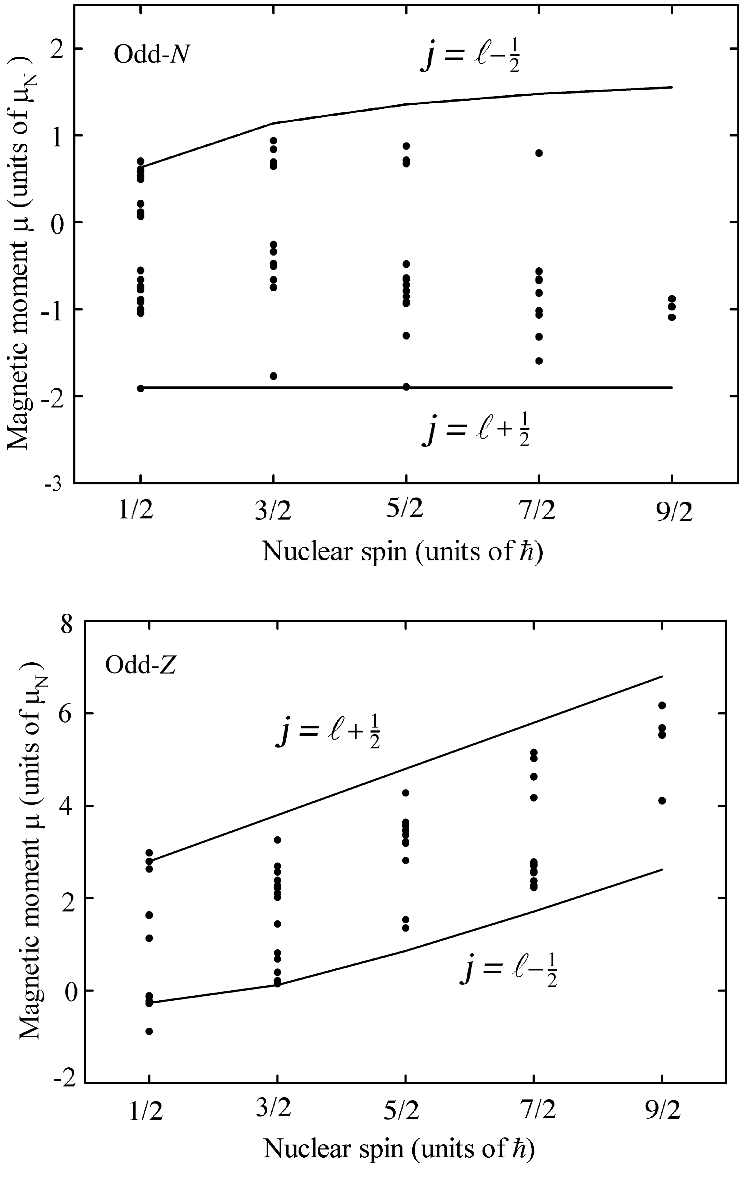

Figure 7.5 Magnetic moments for odd-N, even-Z nuclei (upper diagram) and odd-Z, even-N (lower diagram) as functions of nuclear spin compared with the predictions of the single-particle shell model (the Schmidt lines)

spectrum becomes very complicated because several nucleons can be excited simultaneously into a superposition of many different configurations to produce a given nuclear spin and parity. When trying to predict the first one or two excited states using a filling diagram like Figure 7.4, we are looking for the configuration that is nearest to the ground state configuration. This will normally involve *either* moving an unpaired nucleon to the next highest level, *or* moving a nucleon from the sub-shell below the unpaired nucleon up one level to pair with it. Thus it is necessary to consider levels just above and below the last nucleons (protons and neutrons).

As an example, consider the case of ${}^{17}_{8}\mathrm{O}$. Its ground-state configuration is given in Equations (7.26). All the proton sub-shells are filled, and all the neutrons are in filled sub-shells except for the last one, which is in a sub-shell on its own. There are three possibilities to consider for the first excited state:

1. promote one of the $1p_{\frac{1}{2}}$ protons to $1d_{\frac{5}{2}}$, giving a configuration of $(1p_{\frac{1}{2}})^{-1}(1d_{\frac{5}{2}})^{1}$, where the superscript -1 means that the shell is one particle short of being filled;

2. promote one of the $1p_{\frac{1}{2}}$ neutrons to $1d_{\frac{5}{2}}$, giving a configuration of $(1p_{\frac{1}{2}})^{-1}(1d_{\frac{5}{2}})^{2}$;

3. promote the $1d_{\frac{5}{2}}$ neutron to the next level, which is probably $2s_{\frac{1}{2}}$ (or the nearby $1d_{\frac{3}{2}}$), giving a configuration of $(1s_{\frac{1}{2}})^{1}$ or $(1d_{\frac{3}{2}})^{1}$.

Following the diagram of Figure 7.4, the third of these possibilities would correspond to the smallest energy shift, so it should be favoured over the others. The next excited state might involve moving the last neutron up a further level to $1d_{\frac{3}{2}}$, or putting it back where it was and adopting configurations (1) or (2). Option (2) is favoured over (1) because it keeps the excited neutron paired with another, which should have a slightly lower energy than creating two unpaired protons. When comparing these predictions with the observed excited levels it is found that the expected excited states do exist, but not necessarily in precisely the order predicted.

The shell model has many limitations, most of which can be traced to its fundamental assumption that the nucleons move independently of one another in a spherically symmetric potential. The latter, for example, is only true for nuclei that are close to having doubly-filled magnetic shells and predicts zero electric quadruple moments, whereas in practice many nuclei are deformed and quadruple moments are often substantial. We discuss this important observation in the next section.

7.4 Non-Spherical Nuclei

So far we have discussed only spherical nuclei, but with non-sphericity new phenomena are allowed, including additional modes of excitation and the possibility of an electric quadrupole moment.

7.4.1 Electric quadrupole moments

The charge distribution in a nucleus is described in terms of electric multipole moments and follows from the ideas of classical electrostatics. If we have a localized classical charge distribution with charge density $\rho(\mathbf{x})$ within a volume τ, then the first moment that can be non-zero is the electric quadrupole Q, defined by

$$eQ \equiv \int \rho(\mathbf{x})(3z^2 - r^2)\mathrm{d}^3\mathbf{x}, \tag{7.32}$$

where we have taken the axis of symmetry to be the z-axis. The analogous definition in quantum theory is

$$Q = \frac{1}{e}\sum_i \int \psi^* q_i (3z_i^2 - r^2)\psi \, \mathrm{d}^3\mathbf{x}, \tag{7.33}$$

where ψ is the nuclear wavefunction and the sum is over all relevant nucleons, each with charge q_i.[10] The quadrupole moment is zero if $|\psi|^2$ is spherically symmetric and so a non-zero value of Q would be indicative of a non-spherical nuclear charge distribution.

If we consider a spheroidal distribution with semi-axes defined as in Figure 2.14, then evaluation of Equation (7.32) leads to the result

$$Q_{\text{intrinsic}} = \frac{2}{5}Ze(a^2 - b^2), \tag{7.34}$$

where $Q_{\text{intrinsic}}$ is the value of the quadrupole moment for a spheroid at rest and Ze is its total charge. For small deformations,

$$Q_{\text{intrinsic}} \approx \frac{6}{5}ZeR^2\varepsilon, \tag{7.35}$$

where ε is defined in Equation (2.70) and R is the nuclear radius. Thus, for a prolate distribution $(a > b)$, $Q > 0$ and for an oblate distribution $(a < b)$, $Q < 0$, as illustrated in Figure 7.6. The same results hold in the quantum case.

If the nucleus has a spin J and magnetic quantum number M, then Q will depend on M because it depends on the shape and hence the orientation of the charge distribution. The quadrupole moment is then defined as the value of Q for which M has its maximum value projected along the z-axis. This may be evaluated from Equation (7.33) in the single-particle shell model and without proof we state the resulting prediction that for odd-A, odd-Z nuclei with a single proton having a total angular moment j outside closed sub-shells, the value of Q is given by

$$Q \approx -R^2 \frac{(2j-1)}{2(j+1)}. \tag{7.36}$$

[10]The electric dipole moment $d_z = \frac{1}{e}\sum_i \int \psi^* q_i z_i \psi \, \mathrm{d}\tau$ vanishes because it will contain a sum of terms of the form $\langle \psi_i | z_i | \psi_i \rangle$, all of which are zero by parity conservation.

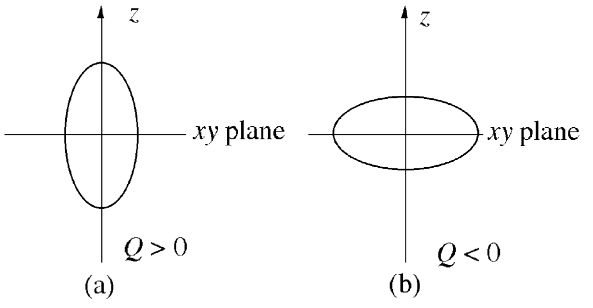

Figure 7.6 Shapes of nuclei leading to (a) $Q > 0$ (prolate), and (b) $Q < 0$ (oblate)

Thus, $Q = 0$ for $j = \frac{1}{2}$. For odd-A, odd-N nuclei with a single neutron outside closed sub-shells Q is predicted to be zero because the neutron has zero electric charge, as will all even-Z, odd-N nuclei because of the pairing effect.

Unlike magnetic dipole moments, electric quadrupole moments are not always well measured and the quoted experimental errors are often far larger than the differences between the values obtained in different experiments. Significant (and difficult to apply) corrections also need to be made to the data to extract the quadrupole moment and this is not always done. The compilation of electric dipole moment data shown in Figure 7.7 is therefore representative. The solid lines are simply to guide the eye and

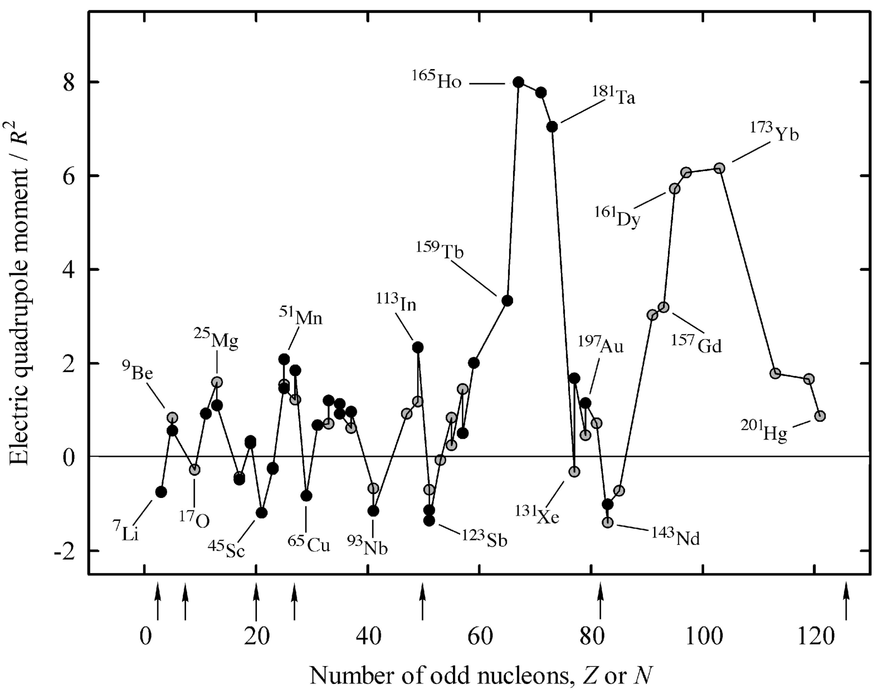

Figure 7.7 Some measured electric quadrupole moments for odd-A nuclei, normalized by dividing by R^2, the squared nuclear radius: grey circles denote odd-N nuclei and black circles odd-Z nuclei; the solid lines have no theoretical significance and the arrows denote the position of closed shells

have no theoretical significance. The arrows indicate the positions of major closed shells. A change of sign of Q at these points is expected because a nucleus with one proton less than a closed shell behaves like a closed-shell nucleus with a negatively charged proton (a proton hole) and there is some evidence for this in the data.

Two features emerge from this diagram. Firstly, while odd-A, odd-Z nuclei with only a few nucleons outside a closed shell do have moments of order $-R^2$, in general the measured moments are larger by factors of two to three and for some nuclei the discrepancy can be as large as a factor of 10. Secondly, odd-A, odd-N nuclei also have non-zero moments, contrary to expectations and, moreover, there is little difference between these and the moments for odd-A, odd-Z nuclei, except that the former tend to be somewhat smaller. These results strongly suggest that for some nuclei it is not a good approximation to assume spherical symmetry and that these nuclei must be considered to have non-spherical mass distributions.

The first attempt to explain the measured electric quadrupole moments in terms of non-spherical nuclei was due to Rainwater. His approach can be understood using the model we discussed in Chapter 2 when considering fission and used above to derive the results of Equations (7.34) and (7.35). There the sphere was deformed into an ellipsoid (see Figure 2.14) with axes parameterized in terms of a small parameter ε via Equation (2.70). The resulting change in the binding energy ΔE_{B} was found to be

$$\Delta E_{\mathrm{B}} = -\alpha\varepsilon^2, \tag{7.37}$$

where

$$\alpha = \frac{1}{5}(2a_s A^{\frac{2}{3}} - a_c Z^2 A^{-\frac{1}{3}}) \tag{7.38}$$

and the coefficients a_s and a_c are those of the SEMF with numerical values given in Equation (2.54). Rainwater assumed that this expression only held for closed-shell nuclei, but not for nuclei with nucleons in unfilled shells. In the latter cases he showed that distortion gives rise to an additional term in ΔE_{B} that is linear in ε, so that the total change in binding energy is

$$\Delta E_{\mathrm{B}} = -\alpha\varepsilon^2 - \beta\varepsilon, \tag{7.39}$$

where β is a parameter that could be calculated from the Fermi energy of the nucleus. This form has a minimum value $\beta^2/4\alpha$ where $\varepsilon = -\beta/2\alpha$. The ground state would therefore be deformed and not spherical.

Finally, once the spin of the nucleus is taken into account in quantum theory, the measured electric quadrupole moment for ground states is predicted to be

$$Q = \frac{j(2j-1)}{(j+1)(2j+1)} Q_{\mathrm{intrinsic}}. \tag{7.40}$$

This model gives values for Q that are of the correct sign, but overestimates them by typically a factor of two. Refined variants of the model are capable of bringing the predictions into agreement with the data by making better estimates of the parameter β.

7.4.2 Collective model

The Rainwater model is equivalent to assuming an *aspherical* liquid drop and Aage Bohr (the son of Neils Bohr) and Mottelson showed that many properties of heavy nuclei could be ascribed to the surface motion of such a drop. However, the single-particle shell model cannot be abandoned because it explains many general features of nuclear structure. The problem was therefore to reconcile the shell model with the liquid-drop model. The outcome is the *collective model*.[11]

This model views the nucleus as having a hard core of nucleons in filled shells, as in the shell model, with outer valence nucleons that behave like the surface molecules of a liquid drop. The motions of the latter introduce non-sphericity in the core that in turn causes the quantum states of the valence nucleons to change from the unperturbed states of the shell model. Such a nucleus can both rotate and vibrate and these new degrees of freedom give rise to rotational and vibrational energy levels. For example, the rotational levels are given by $E_J = J(J+1)\hbar^2/2I$, where I is the moment of inertia and J is the spin of the nucleus. The predictions of this simple model are quite good for small J, but overestimate the energies for larger J. Vibrational modes are due predominantly to *shape oscillations*, where the nucleus oscillates between prolate and oblate ellipsoids. Radial oscillations are much rarer because nuclear matter is relatively incompressible. The energy levels are well approximated by a simple harmonic oscillator potential with spacing $\Delta E = \hbar\omega$, where ω is the oscillator frequency.

In practice, the energy levels of deformed nuclei are very complicated, because there is often coupling between the various modes of excitation, but nevertheless many predictions of the collective model are confirmed experimentally.[12]

7.5 Summary of Nuclear Structure Models

The shell model is based upon the idea that the constituent parts of a nucleus move independently. The liquid-drop model implies just the opposite, since in a drop of incompressible liquid, the motion of any constituent part is correlated with the motion of all the neighbouring pairs. This emphasizes that *models* in physics have a limited domain of applicability and may be unsuitable if applied to a different set of phenomena. As knowledge evolves, it is natural to try and incorporate more

[11] For their development of the collective model, Aage Bohr, Ben Mottelson and Leo Rainwater shared the 1975 Nobel Prize in Physics.
[12] The details are discussed, for example, in Section 2.3 of Je90 and Chapter 17 or Ho97.

phenomena by modifying the model to become more general, until (hopefully) we have a model with firm theoretical underpinning which describes a very wide range of phenomena, i.e. a *theory*. The collective model, which uses the ideas of both the shell and liquid drop models, is a step in this direction. We will conclude this section with a brief summary of the assumptions of each of the nuclear models we have discussed and what each can tell us about nuclear structure.

Liquid-drop model

This model assumes that all nuclei have similar mass densities, with binding energies approximately proportional to their masses, just as in a classical charged liquid drop. The model leads to the SEMF, which gives a good description of the average masses and binding energies. It is largely classical, with some quantum mechanical terms (the asymmetry and pairing terms) inserted in an *ad hoc* way. Input from experiment is needed to determine the coefficients of the SEMF.

Fermi gas model

The assumption here is that nucleons move independently in a net nuclear potential. The model uses quantum statistics of a Fermi gas to predict the depth of the potential and the asymmetry term of the SEMF.

Shell model

This is a fully quantum mechanical model that solves the Schrödinger equation with a specific spherical nuclear potential. It makes the same assumptions as the Fermi gas model about the potential, but with the addition of a strong spin–orbit term. It is able to successfully predict nuclear magic numbers, spins and parities of ground-state nuclei and the pairing term of the SEMF. It is less successful in predicting magnetic moments.

Collective model

This is also a fully quantum mechanical model, but in this case the potential is allowed to undergo deformations from the strictly spherical form used in the shell model. The result is that the model can predict magnetic dipole and electric quadrupole magnetic moments with some success. Additional modes of excitation, both vibrational and rotational, are possible and are generally confirmed by experiment.

It is clear from the above that there is at present no universal nuclear model. What we currently have is a number of models and theories that have limited domains of applicability and even within which they are not always able to explain all the observations. For example, the shell model, while able to give a convincing account of the spins and parities of the ground states of nuclei, is unable to predict the spins of excited states with any real confidence. And of course the shell model has absolutely nothing to say about whole areas of nuclear physics phenomena. Some attempt has been made to combine features of different models, such as is done in the collective model, with some success. A more fundamental theory will require the full apparatus of many-body theory applied to interacting nucleons and some progress has been made in this direction for light nuclei, as we will mention in Chapter 9. A theory based on interacting quarks is a more distant goal.

7.6 α-Decay

To discuss α-decays, we could return to the semiempirical mass formula of Chapter 2 and by taking partial derivatives with respect to A and Z find the limits of α-stability, but the result is not very illuminating. To get a very rough idea of the stability criteria, we can write the SEMF in terms of the binding energy B. Then α-decay is energetically allowed if

$$B(2,4) > B(Z,A) - B(Z-2,A-4). \tag{7.41}$$

If we now make the *approximation* that the line of stability is $Z = N$ (the actual line of stability deviates from this, see Figure 2.7), then there is only one independent variable. If we take this to be A, then

$$B(2,4) > B(Z,A) - B(Z-2,A-4) \approx 4\frac{\mathrm{d}B}{\mathrm{d}A}, \tag{7.42}$$

and we can write

$$4\frac{\mathrm{d}B}{\mathrm{d}A} = 4\left[A\frac{\mathrm{d}(B/A)}{\mathrm{d}A} + \frac{B}{A}\right]. \tag{7.43}$$

From the plot of B/A (Figure 2.2), we have $\mathrm{d}(B/A)/\mathrm{d}A \approx -7.7 \times 10^{-3}\,\mathrm{MeV}$ for $A \geq 120$ and we also know that $B(2,4) = 28.3\,\mathrm{MeV}$, so we have

$$28.3 \approx 4[B/A - 7.7 \times 10^{-3} A], \tag{7.44}$$

which is a straight line on the B/A versus A plot which cuts the plot at $A \approx 151$. Above this value of A, Equation (7.41) is satisfied by most nuclei and α-decay becomes energetically possible.

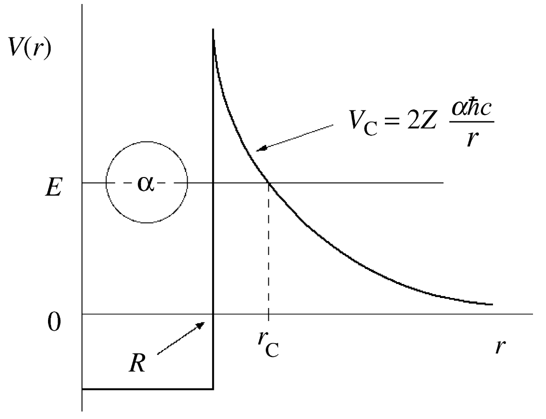

Figure 7.8 Schematic diagram of the potential energy of an α-particle as a function of its distance r from the centre of the nucleus

Lifetimes of α-emitters span an enormous range, and examples are known from 10 ns to 10^{17} years. The origin of this large spread lies in the quantum mechanical phenomenon of *tunelling*. Individual protons and neutrons have binding energies in nuclei of about 8 MeV, even in heavy nuclei (see Figure 2.2), and so cannot in general escape. However, a bound group of nucleons can sometimes escape because its binding energy increases the total energy available for the process. In practice, the most significant decay process of this type is the emission of an α-particle, because unlike systems of two and three nucleons it is very strongly bound by 7 MeV/ nucleon. Figure 7.8 shows the potential energy of an α-particle as a function of r, its distance from the centre of the nucleus.

Beyond the range of the nuclear force, $r > R$, the α-particle feels only the Coulomb potential

$$V_C(r) = \frac{2Z\alpha\hbar c}{r}, \tag{7.45}$$

where we now use Z to be the atomic number of the *daughter* nucleus. Within the range of the nuclear force, $r < R$, the strong nuclear potential prevails, with its strength characterized by the depth of the well. Since the α-particle can escape from the nuclear potential, $E_\alpha > 0$. It is this energy that is released in the decay. Unless E_α is larger than the Coulomb barrier (in which case the decay would be so fast as to be unobservable) the only way the α-particle can escape is by quantum mechanical tunelling through the barrier.

The probability T for transmission through a barrier of height V and thickness Δr by a particle of mass m with energy E_α is given approximately by

$$T \approx e^{-2\kappa\Delta r}, \tag{7.46}$$

where $\hbar\kappa = [2m|V_C - E_\alpha|]^{1/2}$. Using this result, we can model the Coulomb barrier as a succession of thin barriers of varying height. The overall transmission probability is then

$$T = e^{-G}, \tag{7.47}$$

where the *Gamow factor G* is

$$G = \frac{2}{\hbar}\int_R^{r_C} [2m|V_C(r) - E_\alpha|]^{1/2} dr, \tag{7.48}$$

with $\beta = v/c$ and v is the velocity of the emitted particle.[13] This assumes that the orbital angular momentum of the α-particle is zero, i.e. we ignore possible centrifugal barrier corrections.[14] Since r_C is the value of r where $E_\alpha = V_C(r_C)$,

$$r_C = 2Ze^2/4\pi\varepsilon_0 E_\alpha \tag{7.49}$$

and hence

$$V_C(r) = 2Ze^2/4\pi\varepsilon_0 r = r_C E_\alpha/r. \tag{7.50}$$

So, substituting into Equation (7.48) gives

$$G = \frac{2(2mE_\alpha)^{1/2}}{\hbar}\int_R^{r_C} \left[\frac{r_C}{r} - 1\right]^{1/2} dr, \tag{7.51}$$

where m is the reduced mass of the α-particle and the daughter nucleus, i.e. $m = m_\alpha m_D/(m_\alpha + m_D) \approx m_\alpha$. Evaluating the integral in Equation (7.51) gives

$$G = 4Z\alpha\left(\frac{2mc^2}{E_\alpha}\right)^{1/2}\left[\cos^{-1}\sqrt{\frac{R}{r_C}} - \sqrt{\frac{R}{r_C}\left(1 - \frac{R}{r_C}\right)}\right]. \tag{7.52}$$

Finally, since E_α is typically 5 MeV and the height of the barrier is typically 40 MeV, $r_C \gg R$ and from (7.52), $G \approx 4\pi\alpha Z/\beta$, where $\beta = v_\alpha/c$ and v_α is the velocity of the alpha particle within the nucleus.

The probability per unit time λ of the α-particle escaping from the nucleus is proportional to the product of: (a) the probability $w(\alpha)$ of finding the α-particle in the nucleus; (b) the frequency of collisions of the α-particle with the barrier (this

[13] These formulae are derived in Appendix A.
[14] The existence of an angular momentum barrier will suppress the decay rate (i.e. increase the lifetime) compared with a similar nucleus without such a barrier. Numerical estimates of the suppression factors, which increase rapidly with angular momentum, have been calculated by Blatt and Weisskopf and are given in their book B152.

is $v_\alpha/2R$); and (c) the transition probability. Thus, combining these factors, λ is given by

$$\lambda = w(\alpha)\frac{v_\alpha}{2R}\mathrm{e}^{-G} \tag{7.53}$$

and since

$$G \propto \frac{Z}{\beta} \propto \frac{Z}{\sqrt{E_\alpha}}, \tag{7.54}$$

small differences in E_α have strong effects on the lifetime.
To examine this further we can take logarithms of Equation (7.53) to give

$$\log_{10} t_{\frac{1}{2}} = a + bZE_\alpha^{-\frac{1}{2}}, \tag{7.55}$$

where $t_{\frac{1}{2}}$ is the half-life. The quantity a depends on the probability $w(\alpha)$ and so is a function of the nucleus, whereas b is a constant that may be estimated from the above equations to be about 1.7. Equation (7.55) is a form of a relation that was found empirically by Geiger and Nuttall in 1911 long before its theoretical derivation in 1928. It is therefore called the *Geiger-Nuttall relation*. It predicts that for fixed Z, the log of the half-life of α-emitters varies linearly with $E_\alpha^{-\frac{1}{2}}$.

Figure 7.9 shows lifetime data for the isotopes of four nuclei. The very strong variation with α-particle energy is evident; changing E_α by a factor of about 2.5 changes the lifetime by 20 orders of magnitude. In all cases the agreement with the Geiger–Nuttall relation is very reasonable and the slopes are compatible with the

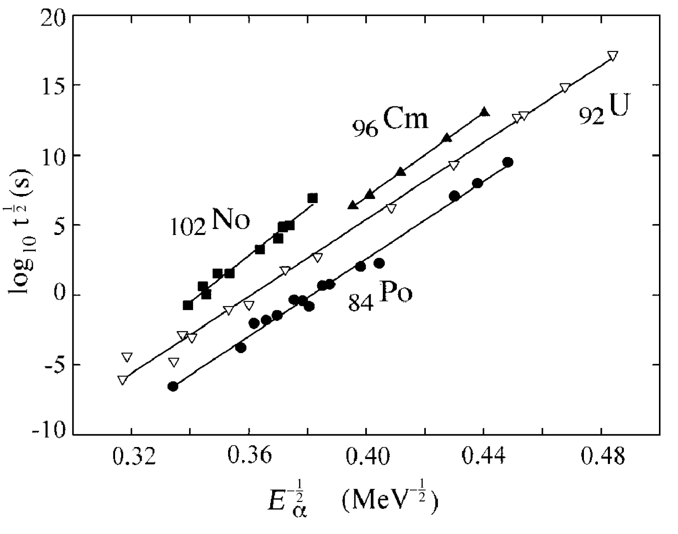

Figure 7.9 Comparison of the Geiger--Nuttall relation with experimental data for some α-emitters

estimate for b above. Thus the simple barrier penetration model is capable of explaining the very wide range of lifetimes of nuclei decaying by α-emission.

7.7 β-Decay

In Chapter 2 we discussed in some detail the phenomenology of β-decay using the SEMF. In this section we return to these decays and examine their theoretical interpretation.

7.7.1 Fermi theory

The first successful theory of nuclear β-decay was proposed in the 1930s by Fermi, long before the *W* and *Z* bosons were known and the quark model formulated. He therefore had to construct a theory based on very general principles, working by analogy with the quantum theory of electromagnetic processes (QED), the only successful theory known at the time for quantum particles.

The general equation for electron β-decay is

$$ {}^{A}_{Z}\mathrm{X} \to {}_{Z+1}^{\;\;A}\mathrm{Y} + e^- + \bar{\nu}_e. \tag{7.56}$$

In Chapter 2, we interpreted this reaction as the decay of a bound neutron, i.e. $n \to p + e^- + \bar{\nu}_e$, and in Chapter 3 we gave the quark interpretation of this decay. In general, it is possible for the internal state of the nucleus to change in other ways during the transition, but we will simplify matters by considering just the basic neutron decay process.

We have also met the Second Golden Rule, which enables transition rates to be calculated provided the interaction is relatively weak. We will write the Golden Rule as

$$\omega = \frac{2\pi}{\hbar}|M_{fi}|^2 n(E), \tag{7.57}$$

where ω is the *transition rate* (probability per unit time), M_{fi} is the *transition amplitude* (also called the *matrix element* because it is one element of a matrix whose elements are all the possible transitions from the initial state *i* to different final states *f* of the system) and $n(E)$ is the *density of states*, i.e. the number of quantum states available to the final system per unit interval of total energy. The density-of-states factor can be calculated from purely kinematical factors, such as energies, momenta, masses and spins where appropriate.[15] The *dynamics* of the process is contained in the matrix element.

[15]This is done explicitly in Appendix A.

The matrix element can in general be written in terms of five basic Lorentz invariant interaction operators, $\hat{\mathrm{O}}$:

$$M_{fi} = \int \Psi_f^*(g\hat{\mathrm{O}})\Psi_i \; \mathrm{d}^3\mathbf{x}, \tag{7.58}$$

where Ψ_f and Ψ_i are total wavefunctions for the final and initial states, respectively, g is a dimensionless coupling constant, and the integral is over three-dimensional space The five categories are called *scalar* (S), *pseudo-scalar* (P), *vector* ($\mathbf{V}$), *axial-vector* ($\mathbf{A}$), and *tensor* (T); the names having their origin in the mathematical transformation properties of the operators. (We have met the **V** and **A** forms previously in Chapter 6 on the electroweak interaction.) The main difference between them is the effect on the spin states of the parent and daughter nuclei. When there are no spins involved, and at low energies, $(g\hat{\mathrm{O}})$ is simply the interaction potential, i.e. that part of the potential that is responsible for the change of state of the system.

Fermi guessed that $\hat{\mathrm{O}}$ would be of the vector type, since electromagnetism is a vector interaction, i.e. it is transmitted by a spin-1 particle – the photon. (Decays of the vector type are called *Fermi transitions*.) We have seen from the work of Chapter 6 that we now know that the weak interaction violates parity conservation and is correctly written as a mixture of both vector and axial-vector interactions (the latter are called *Gamow–Teller transitions* in nuclear physics), but as long as we are not concerned with the spins of the nuclei, this does not make much difference, and we can think of the matrix element in terms of a classical weak interaction potential, like the Yukawa potential. Applying a bit of modern insight, we can assume the potential is of extremely short range (because of the large mass of the W boson), in which case we have seen that we can approximate the interaction by a point-like form and the matrix element then becomes simply a constant, which we write as

$$M_{fi} = \frac{G_\mathrm{F}}{V}, \tag{7.59}$$

where G_F is the Fermi coupling constant we met in Chapter 6. It has dimensions [energy][length]^3 and is related to the charged current weak interaction coupling α_W by

$$G_\mathrm{F} = \frac{4\pi(\hbar c)^3\alpha_\mathrm{W}}{(M_W c^2)^2}. \tag{7.60}$$

In Equation (7.59) it is convenient to factor out an arbitrary volume V, which is used to normalize the wavefunctions. (It will eventually cancel out with a factor in the density-of-states term.)

In nuclear theory, the Fermi coupling constant G_F is taken to be a universal constant and with appropriate corrections for changes of the nuclear state this assumption is also used in β-decay. Experimental results are consistent with the theory under this assumption. However, the theory goes beyond nuclear β-decay, and can be applied to any process mediated by the W boson, provided the energy is not too great. In Chapter 6, for example, we used the same ideas to discuss neutrino scattering. The best process to determine the value of G_{F} is one not complicated by hadronic (nuclear) effects and muon decay is usually used. The lifetime of the muon τ_μ is given to a very good approximation by (ignoring the Cabbibo correction)

$$\frac{1}{\tau_\mu} = \frac{(m_\mu c^2)^5}{192\pi^3 \hbar (\hbar c)^6} G_{\mathrm{F}}^2, \tag{7.61}$$

from which we can deduce that the value of G_{F} is about 90 eV fm^3. It is usually quoted in the form $G_{\mathrm{F}}/(\hbar c)^3 = 1.166 \times 10^{-5}\,\mathrm{GeV}^{-2}$.

7.7.2 Electron momentum distribution

We see from Equation (7.58) that the transition rate (i.e. β-decay lifetime) depends essentially on kinematical factors arising through the density-of-states factor, $n(E)$. To simplify the evaluation of this factor, we consider the neutron and proton to be 'heavy', so that they have negligible kinetic energy, and all the energy released in the decay process goes into creating the electron and neutrino and in giving them kinetic energy. Thus we write

$$E = E_e + E_\nu, \tag{7.62}$$

where E_e is the total (relativistic) energy of the electron, E_ν is the total energy of the neutrino, and E is the total energy released. (This equals $(\Delta m)c^2$, if Δm is the neutron–proton mass difference, or the change in mass of the decaying nucleus.)

The transition rate ω can be measured as a function of the electron momentum, so we need to obtain an expression for the spectrum of β-decay electrons. Thus we will fix E_e and find the differential transition rate for decays where the electron has energy in the range E_e to $E_e + \mathrm{d}E_e$. From the Golden Rule, this is

$$\mathrm{d}\omega = \frac{2\pi}{\hbar} |M|^2 n_\nu (E - E_e) n_e(E_e) \mathrm{d}E_e, \tag{7.63}$$

where n_e and n_ν are the density of states factors for the electron and neutrino, respectively. These may be obtained from our previous result:

$$n(p_e)\mathrm{d}p_e = \frac{V}{(2\pi\hbar)^3} 4\pi p_e^2 \mathrm{d}p_e, \tag{7.64}$$

with a similar expression for n_ν, by changing variables using

$$\frac{\mathrm{d}p}{\mathrm{d}E} = \frac{E}{pc^2}, \tag{7.65}$$

so that

$$n(E_e)\mathrm{d}E_e = \frac{4\pi V}{(2\pi\hbar)^3 c^2} p_e E_e \mathrm{d}E_e, \tag{7.66}$$

with a similar expression for $n(E_\nu)$. Using these in Equation (7.57) and setting $M = G_\mathrm{F}/V$, gives

$$\frac{\mathrm{d}\omega}{\mathrm{d}E_e} = \frac{G_\mathrm{F}^2}{2\pi^3\hbar^7 c^4} p_e E_e p_\nu E_\nu \tag{7.67}$$

where in general

$$p_\nu c = \sqrt{E_\nu^2 - m_\nu^2 c^4} = \sqrt{(E - E_e)^2 - m_\nu^2 c^4}. \tag{7.68}$$

Finally, it is useful to change the variable to p_e by writing

$$\frac{\mathrm{d}\omega}{\mathrm{d}p_e} = \frac{\mathrm{d}E_e}{\mathrm{d}p_e}\frac{\mathrm{d}\omega}{\mathrm{d}E_e} = \frac{G_\mathrm{F}^2}{2\pi^3\hbar^7 c^2} p_e^2 p_\nu E_\nu. \tag{7.69}$$

If we take the antineutrino to be *precisely* massless, then $p_\nu = E_\nu/c$ and Equation (7.69) reduces to

$$\frac{\mathrm{d}\omega}{\mathrm{d}p_e} = \frac{G_\mathrm{F}^2 p_e^2 p_\nu^2}{2\pi^3\hbar^7 c} = \frac{G_\mathrm{F}^2 p_e^2 E_\nu^2}{2\pi^3\hbar^7 c^3} = \frac{G_\mathrm{F}^2 p_e^2 (E - E_\mathrm{e})^2}{2\pi^3\hbar^7 c^3}. \tag{7.70}$$

This expression gives rise to a bell-shaped electron momentum distribution, which rises from zero at zero momentum, reaches a peak and falls to zero again at an electron energy equal to E, as illustrated in the curve labelled $Z = 0$ in Figure 7.10. Studying the precise shape of the distribution near its upper end-point is one way in principle of finding a value for the antineutrino mass. If the neutrino has zero mass, then the gradient of the curve approaches zero at the end-point, whereas any non-zero value results in an end-point that falls to zero with an asymptotically infinite gradient. We will return to this later.

There are several factors that we have ignored or over-simplified in deriving this momentum distribution. The principal ones are to do with the possible changes of nuclear spin of the decaying nucleus, and the electric force acting between the β-particle (electron or positron) and the nucleus. In the first case, when the electron–antineutrino carry away a combined angular momentum of 0 or 1, the

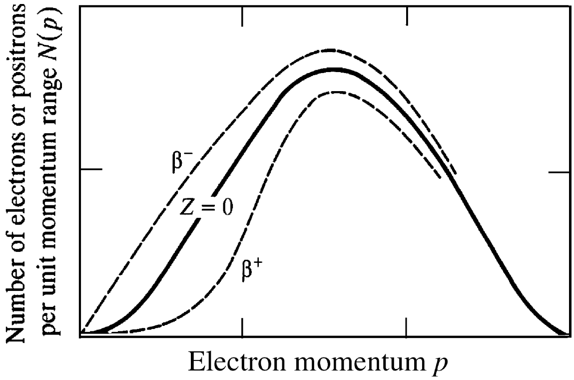

Figure 7.10 Predicted electron spectra: $Z = 0$, without Fermi screening factor; $\beta^{\pm}$, with Fermi screening factor

above treatment is essentially correct: these are the so-called '*allowed transitions*'. However, the nucleus may change its spin by more than 1 unit, and then the simplified short-range potential approach to the matrix element is inadequate. The decay rate in these cases is generally suppressed, although not completely forbidden, despite these being traditionally known as the '*forbidden transitions*'.[16] In the second case, the electric potential between the positive nucleus and a positive β-particle will cause a shift of the low end of its momentum spectrum to the right, since it is propelled away by electrostatic repulsion. Conversely, the low end of the negative β-spectrum is shifted to the left (see Figure 7.10). The precise form of these effects is difficult to calculate, and requires quantum mechanics, but the results are published in tables of a factor $F(Z, E_e)$, called the *Fermi screening factor*, to be applied to the basic β-spectrum.

7.7.3 Kurie plots and the neutrino mass

The usual way of experimentally testing the form of the electron momentum spectrum given by the Fermi theory is by means of a *Kurie plot*. From Equation (7.70), with the Fermi screening factor included, we have

$$\frac{\mathrm{d}\omega}{\mathrm{d}p_e} = \frac{F(Z, E_e) G_{\mathrm{F}}^2 p_e^2 (E - E_e)^2}{2\pi^3 \hbar^7 c^3}, \tag{7.71}$$

which can be written as

$$H(E_e) \equiv \left[\left(\frac{\mathrm{d}\omega}{\mathrm{d}p_e} \right) \frac{1}{p_e^2 K(Z, p_e)} \right]^{\frac{1}{2}} = E - E_e, \tag{7.72}$$

[16]For a discussion of forbidden transitions see, for example, Co01.

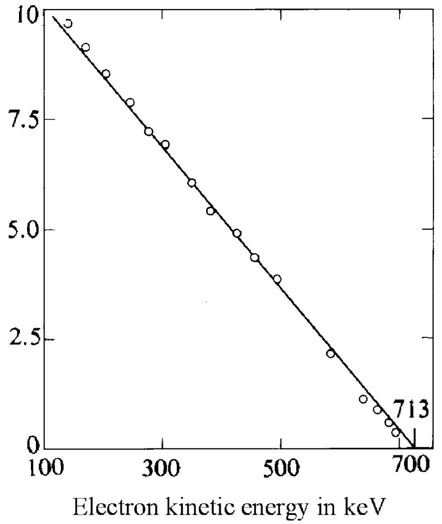

Figure 7.11 Kurie plot for the β-decay of ^{36}Cl (the y-axis is proportional to the function $H(E_e)$ above)

where $K(Z,p_e)$ includes $F(Z,E_e)$ and all the fixed constants in Equation (7.71). A plot of the left-hand side of this equation – using the measured $\mathrm{d}\omega/\mathrm{d}p_e$ and p_e, together with the calculated value of $K(Z,p_e)$ – against the electron energy E_e should then give a straight line with an intercept of E. An example is shown in Figure 7.11.

If the neutrino mass is not exactly zero then it is straightforward to repeat the above derivation and to show that the left-hand side of the Kurie plot is proportional to

$$\{(E-E_e)[(E-E_e)^2 - m_\nu^2 c^4]^{\frac{1}{2}}\}^{\frac{1}{2}}. \tag{7.73}$$

This will produce a *very* small deviation from linearity extremely close to the end-point of the spectrum and the straight line will curve near the end point and cut the axis vertically at $E_0' = E_0 - m_\nu c^2$. In order to have the best conditions for measuring the neutrino mass, it is necessary to use a nucleus where a non-zero mass would have a maximum effect, i.e. the maximum energy release $E = E_0$ should only be a few keV. Also at such low energies atomic effects have to be taken into account, so the initial and final atomic states must be very well understood. The most suitable case is the decay of tritium,

$$^3\mathrm{H} \rightarrow {}^3\mathrm{He} + e^- + \bar{\nu}_e, \tag{7.74}$$

where $E_0 = 18.6\,\mathrm{keV}$. The predicted Kurie plot very close to the end-point is shown in Figure 7.12.

Since the counting rate near E_0 is vanishingly small, the experiment is extremely difficult. In practice, the above formula is fitted to data close to the end-point of the spectrum and extrapolated to E_0. The best experiments are consistent with a zero

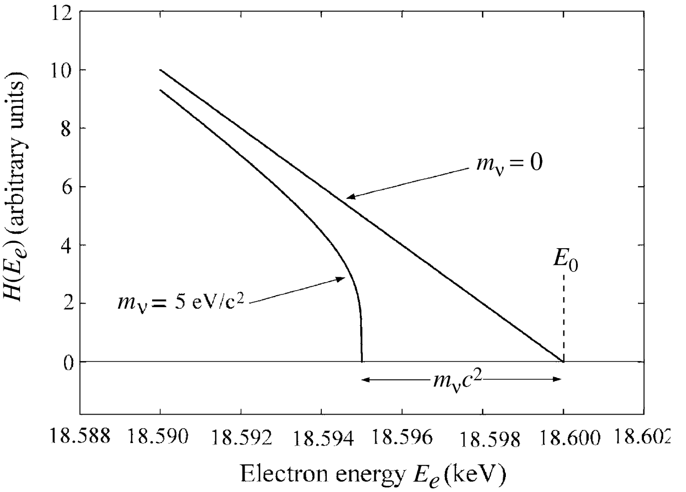

Figure 7.12 Expected Kurie plot for tritium decay very close to the end-point of the electron energy spectrum for two cases: $m_\nu = 0$ and $m_\nu = 5\,\mathrm{eV/c^2}$

neutrino mass, but when experimental and theoretical uncertainties are taken into account, an upper limit of about 2–3 eV/c^2 results.

7.8 γ-Emission and Internal Conversion

In Chapter 2 we mentioned that excited states of nuclei frequently decay to lower states (often the ground state) by the emission of photons in the energy range appropriate to γ-rays and that in addition it is possible for the nucleus to de-excite by ejecting an electron from a low-lying atomic orbit. We shall discuss this only briefly because a proper treatment requires using a quantized electromagnetic radiation field and is beyond the scope of this book. Instead, we will outline the results, without proof.

7.8.1 Selection rules

Gamma emission is a form of electromagnetic radiation and like all such radiation is caused by a changing electric field inducing a magnetic field. There are two possibilities, called electric (E) radiation and magnetic (M) radiation. These names derive from the semiclassical theory of radiation, in which the radiation field arises because of the time variation of charge and current distributions. The classification of the resulting radiation is based on the fact that total angular momentum and parity are conserved in the overall reaction, the latter because it is an electromagnetic process.

The photon carries away a total angular momentum, given by a quantum number L[17], which must include the fact that the photon is a spin-1 vector meson. The minimum value is $L = 1$. This is because a real photon has two possible polarization states corresponding, for example, to $L_z = \pm 1$. Thus in the transition, there must be a change of L_z for the emitting nucleus of ± 1 and this cannot happen if $L = 0$. Hence, if the spins of the initial and final nuclei states are denoted by $\mathbf{J}_i$ and $\mathbf{J}_f$ respectively, the transition $\mathbf{J}_i = \mathbf{0} \rightarrow \mathbf{J}_f = \mathbf{0}$ is strictly forbidden. In general, the photons are said to have a multipolarity L and we talk about multipole radiation; transitions are called dipole $(L = 1)$, quadrupole $(L = 2)$, octupole $(L = 3)$ etc.. Thus, for example, M2 stands for magnetic quadrupole radiation. The allowed values of L are restricted by the conservation equation relating the photon total angular momentum $\mathbf{L}$ and the spins of the initial and final nuclei states, i.e.

$$\mathbf{J}_i = \mathbf{J}_f + \mathbf{L}. \tag{7.75}$$

Thus, L may lie in the range

$$J_i + J_f \geq L \geq |J_i - J_f|. \tag{7.76}$$

It is also necessary to take account of parity. In classical physics, an electric dipole $q\mathbf{r}$ is formed by having two equal and opposite charges q separated by a distance $\mathbf{r}$. It therefore has negative parity under $\mathbf{r} \rightarrow -\mathbf{r}$. Similarly, a magnetic dipole is equivalent to a charge circulating with velocity $\mathbf{v}$ to form a current loop of radius $\mathbf{r}$. The magnetic dipole is then of the form $q\mathbf{r} \times \mathbf{v}$, which does not change sign under a parity inversion and thus has positive parity. The general result, which we state without proof, is that electric multipole radiation has parity $(-1)^L$, whereas magnetic multipole radiation has parity $(-1)^{L+1}$. We thus are led to the selection rules for γ emission shown in Table 7.1. Using this table we can determine which radiation types are allowed for any specific transition. Some examples are shown in Table 7.2.

Table 7.1 Selection rules for γ emission

Multipolarity	Dipole		Quadrupole		Octupole	
Type of radiation	E1	M1	E2	M2	E3	M3
L	1	1	2	2	3	3
ΔP	Yes	No	No	Yes	Yes	No

Although transitions $\mathbf{J}_i = \mathbf{0} \rightarrow \mathbf{J}_f = \mathbf{0}$ are forbidden because the photon is a real particle, such transitions could occur if a *virtual* photon is involved, provided parity does not change. The reason for this is that a virtual photon does not have the

[17] As this is the total angular momentum, logically it would be better to employ the symbol $\mathbf{J}$. However, as $\mathbf{L}$ is invariably used in the literature, it will be used in what follows.

Table 7.2 Examples of nuclear electromagnetic transitions

$j_i^{P_i}$	$J_f^{P_f}$	ΔP	L	Allowed transitions
0^+	0^+	No	–	None
$\frac{1}{2}^+$	$\frac{1}{2}^-$	Yes	1	E1
1^+	0^+	No	1	M1
2^+	0^+	No	2	E2
$\frac{3}{2}^-$	$\frac{1}{2}^+$	Yes	1, 2	E1, M2
2^+	1^+	No	1, 2, 3	M1, E2, M3
$\frac{3}{2}^-$	$\frac{5}{2}^+$	Yes	1, 2, 3, 4	E1, M2, E3, M4

restriction on its states of polarization that a real photon does. In practice, the energy of the virtual photon can be transferred to an orbital atomic electron that can thereby be ejected. This is the process of *internal conversion.* There is another possibility whereby the virtual photon can create an internal e^+e^- pair. This is referred to as *internal pair production.*

7.8.2 Transition rates

In semi-classical radiation theory, the transition probability per unit time, i.e. the emission rate, is given by[18]

$$T_{fi}^{\mathrm{E,M}}(L) = \frac{1}{4\pi\varepsilon_0}\frac{8\pi(L+1)}{L[(2L+1)!!]^2}\frac{1}{\hbar}\left(\frac{E_\gamma}{\hbar c}\right)^{2L+1} B_{fi}^{\mathrm{E,M}}(L), \tag{7.77}$$

where E_γ is the photon energy, E and M refer to electric and magnetic radiation, and for odd-n, $n!! \equiv n(n-2)(n-4)\ldots 3.1$. The function $B_{fi}^{\mathrm{E,M}}(L)$ is the so-called *reduced transition probability* and contains all the nuclear information. It is essentially the square of the matrix element of the appropriate operator causing the transition producing photons with multipolarity L, taken between the initial and final nuclear state wave functions. For electric transitions, B is measured in units of $e^2\,\mathrm{fm}^{2L}$ and for magnetic transitions in units of $(\mu_\mathrm{N}/c)^2\mathrm{fm}^{2L-2}$ where μ_N is the nuclear magneton.

To go further requires knowledge of the nuclear wave functions. An approximation due to Weisskopf is based on the single-particle shell model. This approach assumes that the radiation results from the transition of a single proton from an initial orbital state of the shell model to a final state of zero angular momentum. In this model the general formulas reduce to

$$B^{\mathrm{E}}(L) = \frac{e^2}{4\pi}\left(\frac{3R^L}{L+3}\right)^2 \tag{7.78a}$$

[18]See, for example, Chapter 16 of Ja75.

for electric radiation and

$$B^{\mathrm{M}}(L) = 10\left(\frac{\hbar}{m_{\mathrm{p}}cR}\right)^2 B^E(L) \tag{7.78b}$$

for magnetic radiation, where R is the nuclear radius and m_{p} is the mass of the proton. Finally, from the work in Chapter 2 on nuclear sizes, we can substitute $R = R_0A^{1/3}$, with $R_0 = 1.21\,\mathrm{fm}$, to give the final results:

$$B^{\mathrm{E}}(L) = \frac{e^2}{4\pi}\left(\frac{3}{L+3}\right)^2 (R_0)^{2L}A^{2L/3} \tag{7.79a}$$

and

$$B^{\mathrm{M}}(L) = \frac{10}{\pi}\left(\frac{e\hbar}{2m_{\mathrm{p}}c}\right)^2\left(\frac{3}{L+3}\right)^2 (R_0)^{2L-2}A^{(2L-2)/3}. \tag{7.79b}$$

Figure 7.13 shows an example of the transition rates $T^{\mathrm{E,M}}$ calculated from Equation (7.77) using the approximations of Equations (7.79). Although these are only approximate predictions, they do confirm what is observed experimentally: for a given transition there is a very substantial decrease in decay rates with increasing L, and electric transitions have decay rates about two orders of magnitude higher than the corresponding magnetic transitions.

Finally, it is often useful to have simple formulas for *radiative widths* Γ_γ. These follow from Equations (7.77), (7.78) and (7.79) and for the lowest multipole transitions may be written

$$\Gamma_\gamma(\mathrm{E1}) = 0.068E_\gamma^3A^{2/3}; \quad \Gamma_\gamma(\mathrm{M1}) = 0.021E_\gamma^3; \quad \Gamma_\gamma(\mathrm{E2}) = (4.9\times 10^{-8})E_\gamma^5A^{4/3}, \tag{7.80}$$

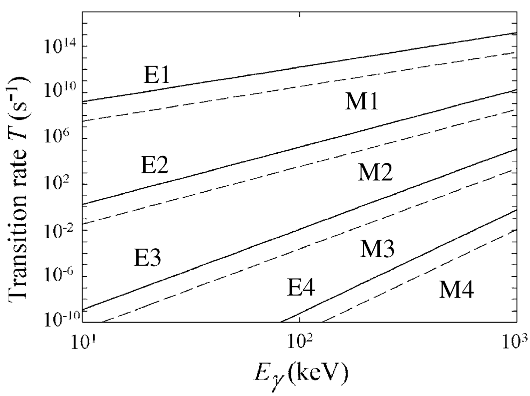

Figure 7.13 Transition rates using single-particle shell model formulas of Weisskopf as a function of photon energy for a nucleus of mass number $A = 60$

where Γ_γ is measured in eV, the transition energy E_γ is measured in MeV and A is the mass number of the nucleus. These formulae are based on the single-particle approximation and in practice collective effects often give values that are much greater than those predicted by Equations (7.80).

Problems

7.1 Assume that in the shell model the nucleon energy levels are ordered as shown in Figure 7.4. Write down the shell-model configuration of the nucleus ${}^7_3\mathrm{Li}$ and hence find its spin, parity and magnetic moment (in nuclear magnetons). Give the two most likely configurations for the first excited state, assuming that only protons are excited.

7.2 A certain odd-parity shell-model state can hold up to a maximum of 16 nucleons; what are its values of j and ℓ?

7.3 The ground state of the radioisotope ${}^{17}_9\mathrm{F}$ has spin-parity $j^P = \frac{5}{2}^+$ and the first excited state has $j^P = \frac{1}{2}^-$. By reference to Figure 7.4, suggest two possible configurations for the latter state.

7.4 What are the configurations of the ground states of the nuclei ${}^{93}_{41}\mathrm{Nb}$ and ${}^{33}_{16}\mathrm{S}$ and what values are predicted in the single-particle shell model for their spins, parities and magnetic dipole moments?

7.5 Show explicitly that a uniformly charged ellipsoid at rest with total charge Ze and semi-axes defined in Figure 2.14, has a quadrupole moment $Q = \frac{2}{5}Ze(a^2 - b^2)$.

7.6 The ground state of the nucleus ${}^{165}_{67}\mathrm{Ho}$ has an electric quadrupole moment $Q \approx 3.5\,\mathrm{b}$. If this is due the fact that the nucleus is a deformed ellipsoid, use the result of Question 7.5 to estimate the sizes of its semi-major and semi-minor axes.

7.7 The decay ${}^{244}_{98}\mathrm{Cf}(0^+) \to {}^{240}_{96}\mathrm{Cm}(0^+) + \alpha$ has a Q-value of 7.329 MeV and a half-life of 19.4 mins. If the frequency and probability of forming α-particles (see Equation (7.53)) for this decay are the same as those for the decay ${}^{228}_{90}\mathrm{Th}(0^+) \to {}^{224}_{88}\mathrm{R}(0^+) + \alpha$, estimate the half-life for the α-decay of ${}^{228}_{90}\mathrm{Th}$, given that its Q-value is 5.520 MeV.

7.8 The hadrons Σ^0 and Δ^0 can both decay via photon emission: $\Sigma^0(1193) \to \Lambda(1116) + \gamma$ (branching ratio ~ 100 per cent); $\Delta^0(1232) \to n + \gamma$ (branching ratio 0.56 per cent). If the lifetime of the Δ^0 is 0.6×10^{-23} s, estimate the lifetime of the Σ^0.

7.9 The reaction ${}^{34}\mathrm{S}(p, n){}^{34}\mathrm{Cl}$ has a threshold proton laboratory energy of 6.45 MeV. Calculate non-relativistically the upper limit of the positron energy in the β-decay of ${}^{34}\mathrm{Cl}$, given that the mass difference between the neutron and the hydrogen atom is 0.78 MeV.

7.10 To determine the mass of the electron neutrino from the β-decay of tritium requires measurements of the electron energy spectrum very close to the end-point where there is a paucity of events (see Figure 7.12.). To see the nature of the problem, estimate the fraction of electrons with energies within 10 eV of the end-point.

7.11 The electron energy spectra of β-decays with very low-energy end-points E_0 may be approximated by $\mathrm{d}\omega/\mathrm{d}E = E^{1/2}(E_0 - E)^2$. Show that in this case the mean energy is $\frac{1}{3}E_0$.

7.12 The ground state of $^{35}_{73}\mathrm{Br}$ has $J^P = \frac{1}{2}^-$ and the first two excited states have $J^P = \frac{5}{2}^-(26.92\,\mathrm{keV})$ and $J^P = \frac{3}{2}^-(178.1\,\mathrm{keV})$. List the possible γ-transitions between these levels and estimate the lifetime of the $\frac{3}{2}^-$ state.

7.13 Use the Weisskopf formulas of Equations (7.79) to calculate the radiative width $\Gamma_\gamma(\mathrm{E3})$ expressed in a form analogous to Equations (7.80).